Ta-Doped Charge-Transferring Ir Shells on Ru Cores: Dual Stabilisation and Synergistic OER Catalysis for PEMWE

Han Wang[a], Tianxi Wen[a], Xinyi Gong[c], Mingjun Ren[c], Qunli Tang[a], Aiping Hu[a], Xiaohua Chen[a,], and Liangliang Zou[b]**

[A] *College of Materials Science and Engineering, Hunan Province Key Laboratory for Advanced Carbon Materials and Applied Technology, Hunan University, Changsha 410082, P. R.*

[b] *School of Materials Science and Engineering, Suzhou University of Science and Technology, Suzhou, 215009, China.*

[c] *Suzhou Bohydrogen New Energy Technology Co., Ltd, Suzhou, 215009, China.*

E-mail address: xiaohuachen@hnu.edu.cn (X. Chen), zoull@usts.edu.cn (L. Zou).

Experimental Methods

Material Synthesis: The Ta-IrRuOx@IrOx catalyst was synthesized via a stepwise selective reduction-deposition anchoring strategy. Briefly, carbon powder and MgO hard templates were first dispersed in an isopropanol water mixture using an ultra-high-power dispersing rod to achieve uniform distribution. Subsequently, 0.1871 g of chloroiridic acid ($H_2IrCl_6 \cdot 3H_2O$) and 0.5612 g of ruthenium chloride (anhydrous $RuCl_3$) were added and thoroughly dispersed under an inert atmosphere, followed by the slow dropwise addition of a tantalum pentachloride ($TaCl_5$) alcohol solution (0.0073 g of $TaCl_5$ in total). The mixture was then heated at 90 °C for 2 h to facilitate the reduction and precursor formation.

Afterward, the pH of the system was adjusted to 8 with potassium hydroxide (KOH) solution, and a diluted solution of 0.3742 g of chloroiridic acid ($H_2IrCl_6 \cdot 3H_2O$) was carefully injected via a microsyringe to induce secondary precipitation. The product was collected by centrifugation, washed repeatedly with water, dried under vacuum at 80 for 12 h, and then uniformly mixed with sodium nitrate. Finally, the sample was annealed in air at 450 for 4 h, followed by thorough washing with dilute hydrochloric acid and deionized water for several times.

For comparison, the reference catalysts IrRuOx@IrOx and Ta-IrRuOx were synthesized by the same procedure: the former was prepared without the addition of tantalum pentachloride, while the latter excluded the secondary chloroiridic acid deposition step.

Characterisations: X-ray powder diffraction (XRD) patterns were recorded on a Rigaku D/Max-2500 diffractometer with Cu Kα radiation at a scan rate of 10° min^{-1} over the 2θ range of 10° to 90°. The surface morphologies and elemental distributions of the samples were characterised via a JEOL JSM 7500F scanning electron microscope (SEM) and a Talos F200X G2 AEMC field-emission transmission electron microscope (TEM). Electron paramagnetic resonance (EPR) measurements were performed on a Bruker E580-10/12 spectrometer at 100 K. X-ray photoelectron spectroscopy (XPS) analysis was carried out using a Thermo Scientific ESCALAB 250Xi spectrometer to determine the chemical states of the products. The elemental contents of the samples were quantified by an Agilent 5110 inductively coupled plasma optical emission spectrometer (ICP-OES).

Electrochemical measurements in a three-electrode cell: Electrochemical measurements were performed in a standard three-electrode cell, wherein a carbon rod and a mercury/mercurous sulfate (Hg/Hg_2SO_4) electrode functioned as the counter and reference electrodes, respectively. All experiments utilised a glassy carbon electrode (GCE) with a diameter of 3 mm and a geometric area of 0.0707 cm^2 as the working electrode; all apparent current densities cited herein were calculated based on this geometric area. An electrochemical workstation (CHI730E) was used to control current and voltage during measurements. Before testing, the GCE was sequentially polished with 500 nm and 30 nm alumina powders until a mirror-like finish was obtained. For catalyst ink preparation, 10 mg of the synthesised catalyst was dispersed in a mixture comprising 2500 μL of ultrapure deionised water, 300 μL of isopropanol, and 200 μL

of Nafion (5 wt%), followed by ultrasonication for 1 hour. An appropriate volume of the resulting homogenous ink was subsequently cast onto the polished GCE to serve as the working electrode. During linear sweep voltammetry (LSV), cyclic voltammetry (CV), and chronopotentiometry (CP) measurements, the electrolyte was stirred at 300 rpm using an external magnetic stirrer to prevent visible oxygen bubbles from forming on the GCE surface. LSV measurements were conducted in nitrogen-saturated 0.5 M H_2SO_4 aqueous solution at a scan rate of 5 mV s^{-1}, covering a potential range from 0.6 to 0.9 V versus the reversible hydrogen electrode (RHE), with the GCE rotating at a consistent speed of 1600 rpm. For CP measurements at a current density of 10 mA cm^{-2}, the working electrode was prepared by spray-coating the homogeneous catalyst ink onto a 1×1 cm^2 carbon paper, with the catalyst loading optimised for the specific test.

Mass activity calculation: The mass activity (jmass) of Ta-IrRuOx@IrOx was determined using the following equation:

$$j_{mass} = \frac{i_{geo}}{m_{cat} \times Ir\ wt\%}$$

where i_{geo} is the geometric current (A) obtained from LSV, m_cat is the loading of catalysts on the electrode, and Ir wt% is the mass ratio of Ir in Ta-IrRuOx@IrOx, which is calculated from the results of ICP-OES.

Calculation of the TOF: The TOF of Ta-IrRuOx@IrOx was calculated based on the following equation:

$$TOF = \frac{n_{O_2}}{n_{(Ir+Ru)}}$$

where $n(O_2)$ is the number of oxygen molecules per second, n((Ir+Ru)) is the number of Ir and Ru participating in the OER. In this work, all Ir and Ru on the electrode are assumed to be the active centres for OER. Thus, the n((Ir+Ru)) can be calculated as:

$$n(Ir/Ru) = \frac{m_{cat} \times (Ir/Ru)wt\%}{M_{Ir/Ru}}$$

in which M(Ir/Ru) is the molar mass of Ru (101.07 g mol−1) and Ir (192.22 g mol−1). m_{cat} and (Ir/Ru) wt% are the same as those.

The $n(O_2)$ were calculated from the LSV curve by the following equation:

$$n_{O_2} = \frac{i_{geo}}{z * F}$$

where igeo is the geometric current (A), z is the number of electrons required per oxygen molecule, and F is the Faraday constant (96,484 C mol^{-1}).

Determine the ECSA of Ta-IrRuOx@IrOx: The ECSAs were obtained from the electrochemical double-layer capacitance of the catalytic surface. The electrical double-

layer capacitor (CDL) was measured from double-layer charging curves obtained by cyclic voltammetry in the non-Faradaic region at scan rates from 5 to 25 mV s^{-1}. The following equation measured the CDL:

$$j = \nu C_{DL}$$

where j is the no-Faradaic capacitive current obtained from the CV curve, and ν is the scan rate. The slope of the j-ν curve is regarded as CDL. The ECSA is calculated from the double-layer capacitance according to:

$$ECSA = \frac{C_{DL}}{C_s}$$

Where CS is the specific capacitance of the sample (set as 0.035 mF cm^{-2} according to the previous reports).

DFT calculations: All DFT calculations are performed using the Vienna Ab initio Simulation Package (VASP) with the projector augmented wave (PAW) method. The exchange functional is treated using the generalised gradient approximation (GGA) with the Perdew-Burke-Ernzerhof (PBE) functional. The energy cutoff for the plane wave basis expansion was set to 400 eV. Partial occupancies of the Kohn−Sham orbitals were allowed using the Gaussian smearing method and a width of 0.2 eV. The self-consistent calculations use a convergence energy threshold of 10^-5 eV, and the force convergence was set to 0.05 eV/Å. The k-point of 3×2×1 was used in all the (110) surface calculations. The free energy corrections were considered at the temperature of 298 K, following:

$$\Delta G = \Delta E + \Delta G_{ZPE} + \Delta G_U - T\Delta S$$

where ΔE, ΔG_ZPE, ΔG_U, and ΔS refer to the DFT calculated energy change, the correction from zero-point energy, the correction from inner energy and the correction from entropy. The reaction free energies of the relevant steps were calculated using the computational hydrogen electrode (CHE) model. The solvent effect was accounted for by stabilisation of the adsorbate via the H-bond network in water, yielding stabilisation energies of -0.17 and -0.20 eV for OH* and OOH*, respectively.

First-principles geometry optimisation calculations were carried out within density-functional theory (DFT), implemented in the Vienna Ab Initio Simulation Package (VASP), using the frozen-core projector augmented-wave (PAW) method to describe the interaction between atomic cores and the valence electron density. The exchange-correlation potential was approximated using the generalised gradient approximation (GGA) with the Perdew-Burke-Ernzerhof (PBE) functional. The dispersion-corrected DFT-D3 scheme was employed to describe the Van der Waals (vdW) interactions. Plane-wave cutoff energy was set to 450 eV. The conjugate gradient algorithm was used for ionic optimisation. The convergence thresholds were set to 10-5 eV atom-1 for electronic relaxation and 0.02 eV Å−1 for the Hellmann–Feynman force on each atom. The Brillouin zone in reciprocal space was sampled by a Γ-centered Monkhorst–Pack scheme with 3 × 3 × 1 k-point grids for IrO_2 geometry optimisation. A 15 Å vacuum layer was added to the slab model of IrO_2.

Electrochemical measurements in PEM electrolysis: Membrane electrode assemblies (MEAs) were fabricated with Ta-IrRuOx@IrOx, IrRuOx@IrOx and IrO_2 as anode catalysts and commercial 40 wt% Pt/C as the cathode catalyst. Anode and cathode inks were prepared by dispersing the respective catalysts in 1:1 isopropanol/deionised water, adding 5 wt% Nafion® solution to achieve 20 wt% ionomer content, and sonicating for ≥1 h in an ice-water bath to form homogeneous inks. The inks were sprayed onto HPM2080 membranes, which were hot-pressed at 120 °C under 6 MPa for 5 min; after cooling, the surface PTFE was peeled off to obtain catalyst-coated membranes (CCMs), with anode Ir loading and cathode Pt loading both fixed at 0.3 mg cm^{-2}. CCMs were stored in distilled water for subsequent use.

For PEMWE assembly, 1 mm-thick Ti felt coated with 0.2 μm Pt (anode) and unplatinized Ti felt (cathode) served as porous transport layers (PTLs); the fixture was tightened to 2 N m, with a defined active area of 4 cm^2 (1.95 cm-diameter Ti felt-covered circle). PEMWE performance was tested on a BTS-4000 (NEWARE, China) at 65 °C, with Milli-Q water circulated via a peristaltic pump at 28 mL min^{-1}. Polarisation curves were collected from 0.1 to 5 A cm^{-2}, and long-term stability was evaluated by chronoamperometry at 2 A cm^{-2} (28 mL min^{-1} flow rate for 1 A cm^{-2} polarisation and stability tests).

Estimation of the hydrogen produced and the cost in PEMWE

$$\text{Mass of } H_2 = \frac{j(\text{current density}) \times A(\text{electrolyzer area}) \times t(\text{working time}) \times Mc}{2 \times F}$$

$$= \frac{2\ \text{A cm}^{-2} \times 9\ \text{cm}^2 \times 2000 \times 3600\ \frac{\text{s}}{\text{hours}} \times 2\ \text{g mol}^{-1}}{2 \times 96485\ \text{c mol}^{-1}} = 1343.21\text{g}$$

$$\text{Volume of } H_2 = \frac{m}{\rho} = \frac{1343.21\ \text{g}}{0.09\ \text{g L}^{-1}} = 14924.59\ \text{L}$$

$$\text{Energy consumption} = \frac{1.6855\ \text{V} \times 18\ \text{A} \times 2000\ \text{hours}}{0.69959\ \text{kg}} = \frac{45.173\ \text{kWh}}{\text{kg } H_2} = \frac{4.065\ \text{kWh}}{\text{m}^3\ H_2}$$

$$\text{Cost per kilogram of } H_2 = \text{energy consumption} \times \text{electricity bill}$$

$$= \frac{45.173\ \text{kWh}}{\text{kg } H_2} \times \frac{\text{USD } 0.02}{\text{kWh}} = \frac{\text{USD } 0.903}{\text{kg } H_2}$$

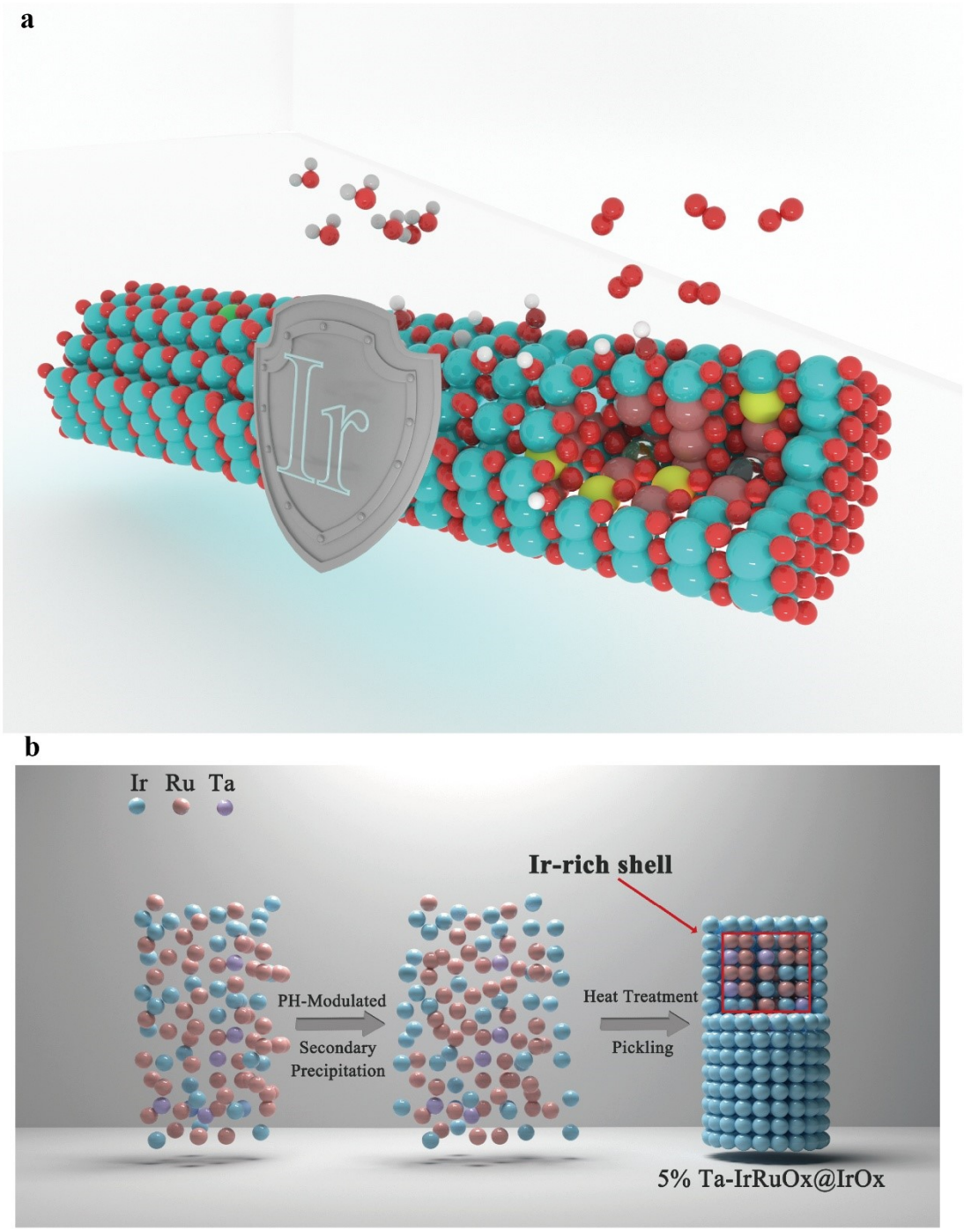

Figure S1. (a) Schematic illustration of the protective effect of the Ir-rich shell in Ta-IrRuOx@IrOx nanorods. (b) Schematic of the synthetic process for 5% Ta-IrRuOx@IrOx core-shell nanorods.

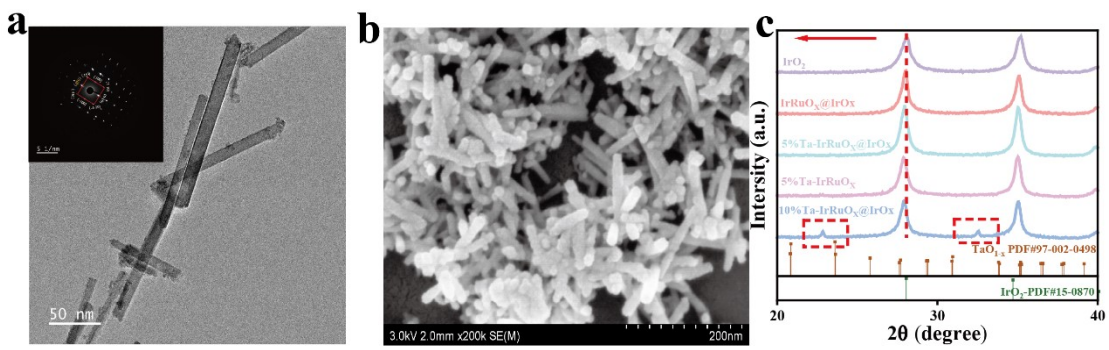

Figure S2. (a) TEM image of the as-prepared nanorods. (b) SEM image of the as-prepared nanorods. (c) XRD patterns of the samples.

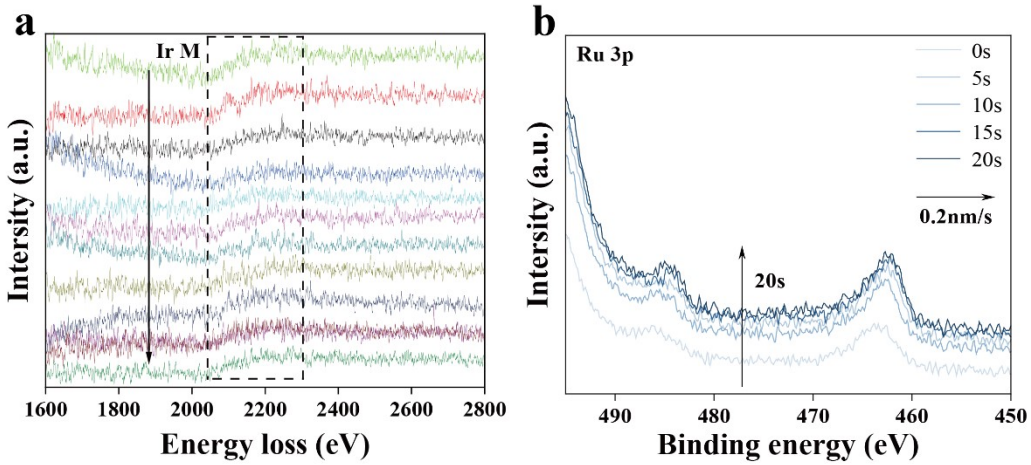

Figure S3. (a) Electron energy loss spectroscopy (EELS) spectra showing the Ir M-edge. (b) X-ray photoelectron spectroscopy (XPS) spectra of the Ru 3p region at different times.

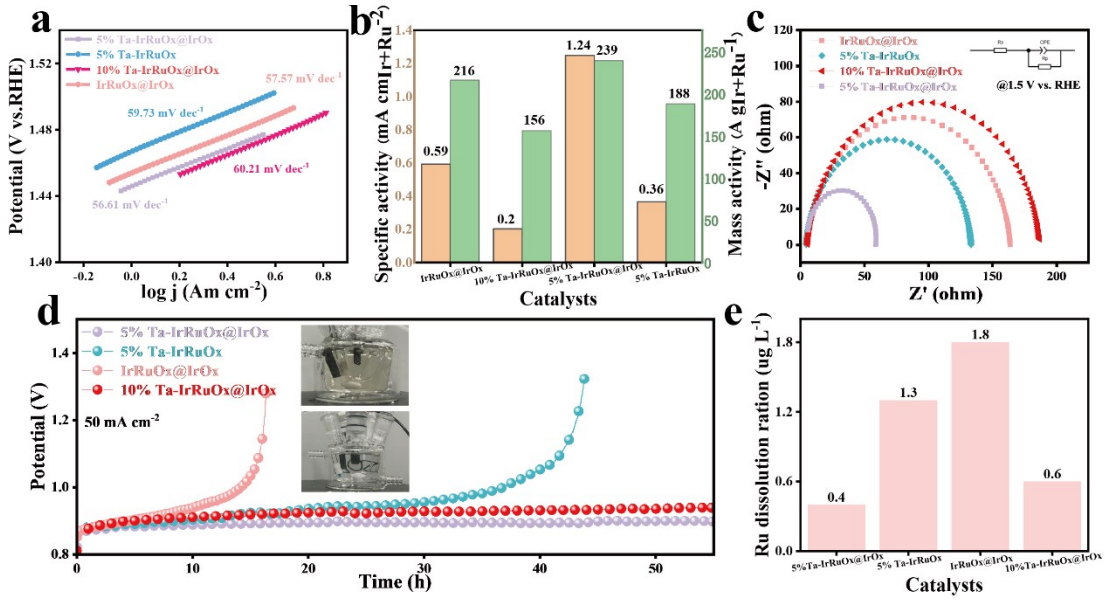

Figure S4. (a) Linear sweep voltammetry (LSV) curves of the catalysts. (b) Specific and mass activity of different catalysts. (c) Electrochemical impedance spectroscopy (EIS) Nyquist plots. (d) Chronopotentiometry curves of the catalysts at 50 mA cm^{-2}. (e) Ru dissolution ratios of the catalysts after stability tests.

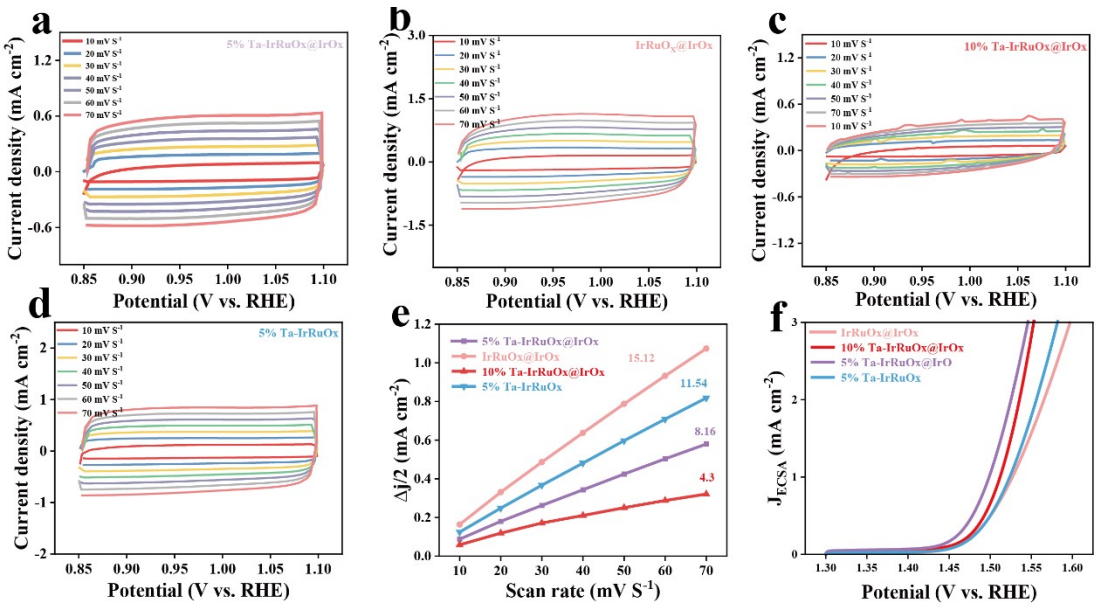

Figure S5. (a-d) Cyclic voltammetry (CV) curves of different catalysts at various scan rates. (e) Double-layer capacitance (Cdl) of the catalysts as a function of scan rate. (f) Without iR-corrected polarization curves normalized by ECSA.

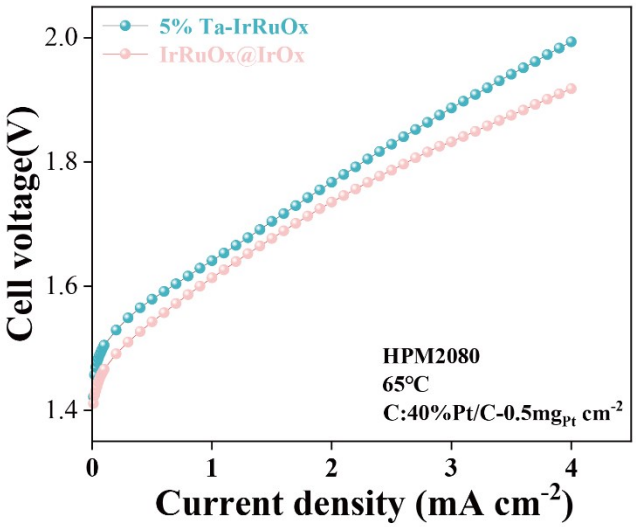

Figure S6. Cell voltage versus current density curves of 5% Ta-IrRuOx and IrRuOx@IrOx catalysts tested under conditions of HPM2080, 65°C, and C:40%Pt/C-0.5mg$_{pt}$ cm^{-2}.

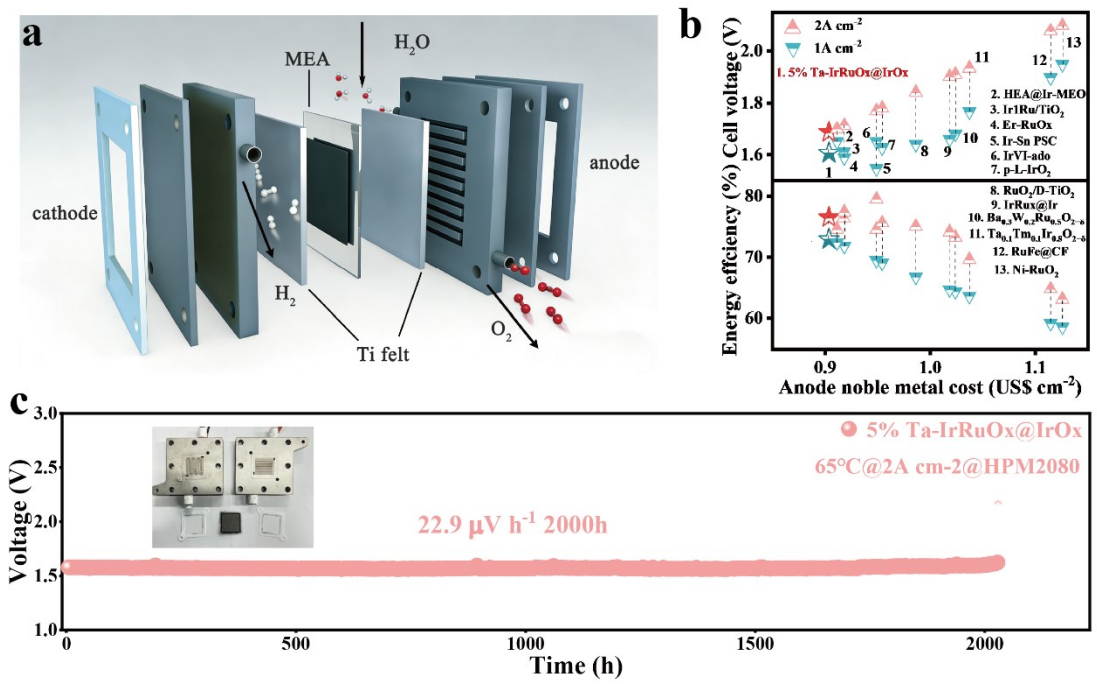

Figure S7. (a) Exploded view of the electrolyser cell configuration. (b) Comparison of cell voltage, energy efficiency, and anode noble metal cost for different catalysts. (c) Long-term stability test of 5% Ta-IrRuOx@IrOx at 65°C and 2 A cm^{-2}, showing a voltage degradation rate of 22.9 μV h^{-1} over 2000 h.

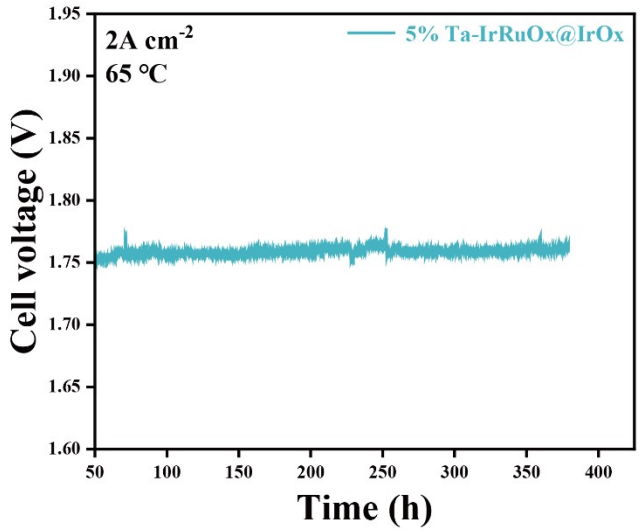

Figure S8. Long-term stability test of 5% Ta-IrRuOx@IrOx catalyst, showing cell voltage as a function of time at 2 A cm^{-2} and 65 °C.

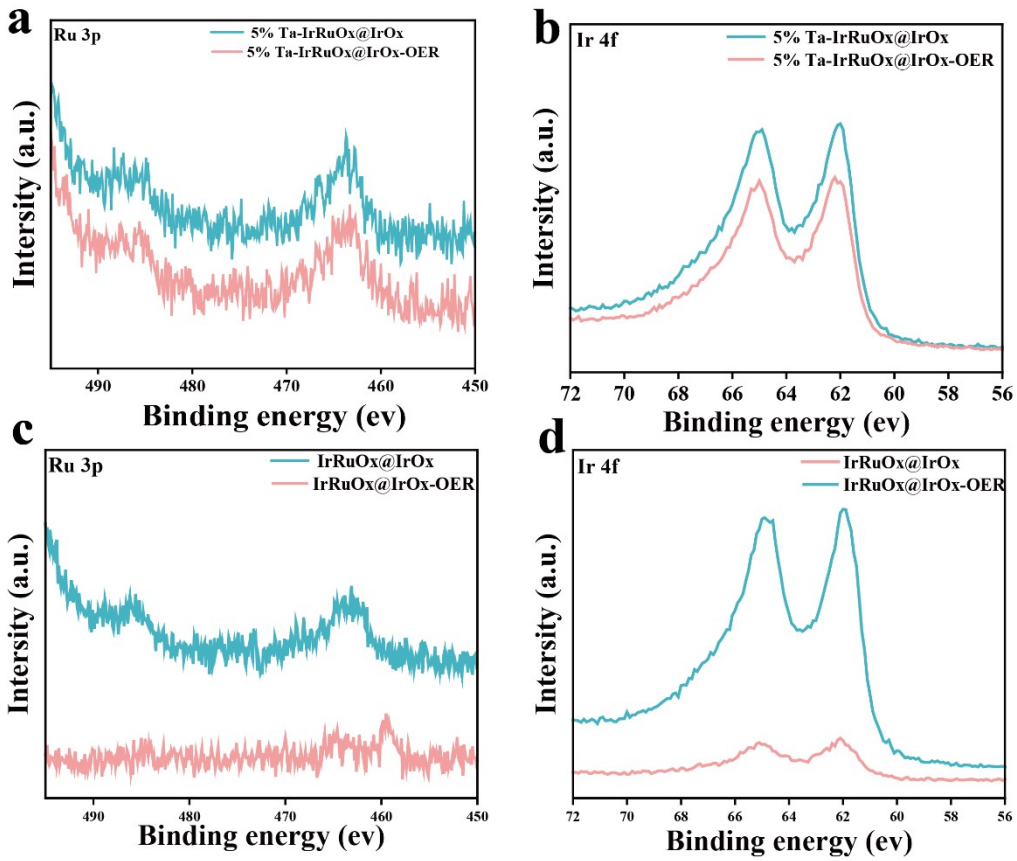

Figure S9. (a-b) XPS spectra of Ru 3p (a) and Ir 4f (b) for 5% Ta-IrRuOx@IrOx. (c-d) Ru 3p (c) and Ir 4f (d) for IrRuOx@IrOx, acquired before (cyan lines) and after (red lines) the OER stability test.

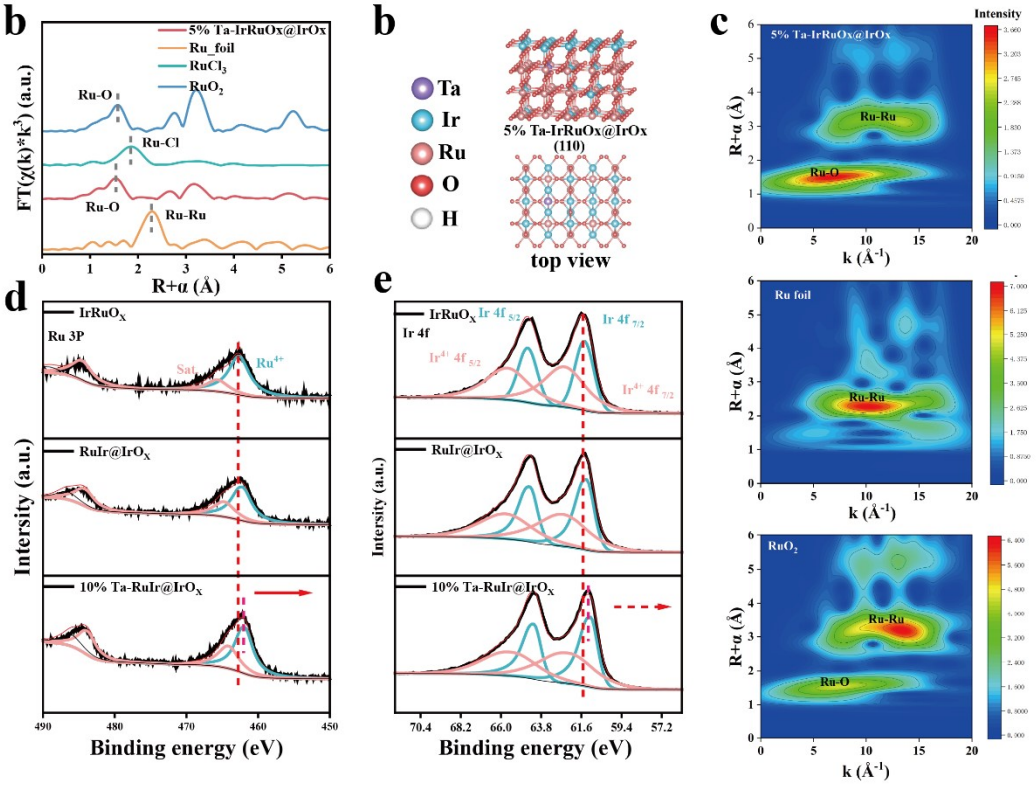

Figure S10. (a) Fourier-transformed extended X-ray absorption fine structure (EXAFS) spectra of the Ru K-edge. (b) Crystal structure model of 5% Ta-IrRuOx@IrOx (top view). (c, f) Wavelet transform plots of the Ru K-edge for different catalysts. (d, e) X-ray photoelectron spectroscopy (XPS) spectra of (d) Ru 3p and (e) Ir 4f regions for other catalysts.

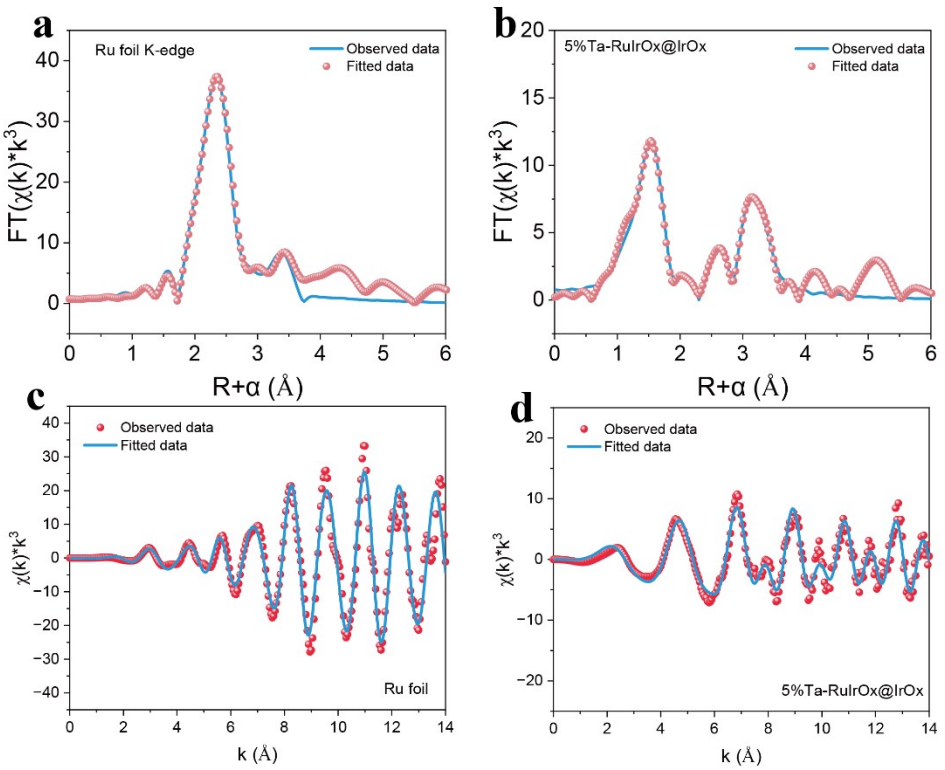

Figure S11. (a, b) Fourier-transformed (FT) k3-weighted extended X-ray absorption fine structure (EXAFS) spectra at Ru K-edge for Ru foil (a) and 5% Ta-IrRuOx@IrOx (b). (c, d) k3-weighted x(k) oscillation curves at Ru K-edge for Ru foil (c) and 5% Ta-IrRuOx@IrOx (d), where red dots represent experimental data and blue lines denote fitted results.

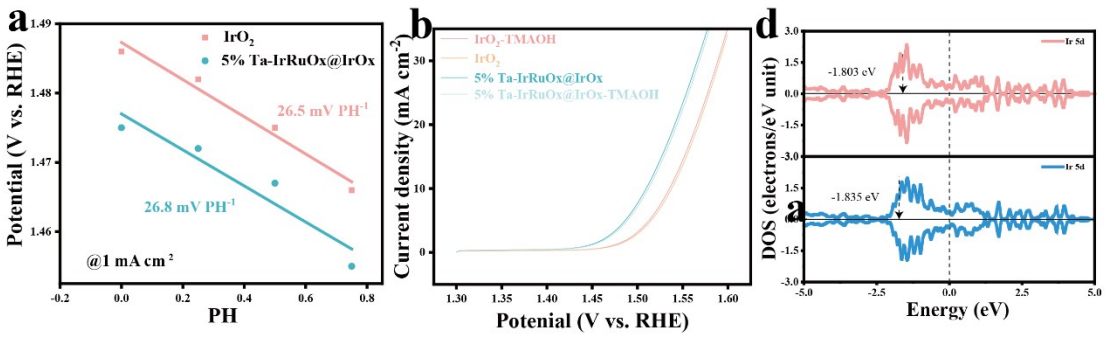

Figure S12. (a) Effect of pH on the potential of IrO_2 and 5% Ta-IrRuOx@IrOx catalysts at 1 mA cm^{-2}. (b) Linear sweep voltammetry (LSV) curves of different catalysts. (d) Density of states (DOS) plots of the catalysts.

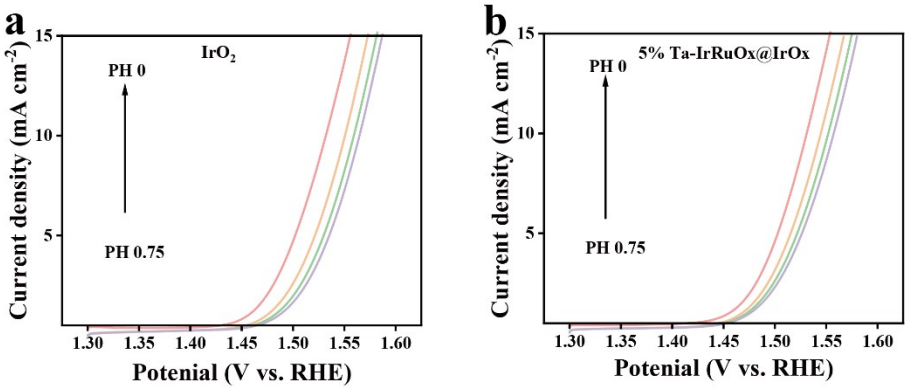

Figure S13. (a) Linear sweep voltammetry (LSV) curves of IrO_2 catalyst for OER at different pH values (pH = 0 and 0.75); (b) Linear sweep voltammetry (LSV) curves of 5% Ta-doped IrRuOx@IrOx catalyst for OER at different pH values (pH = 0 and 0.75).

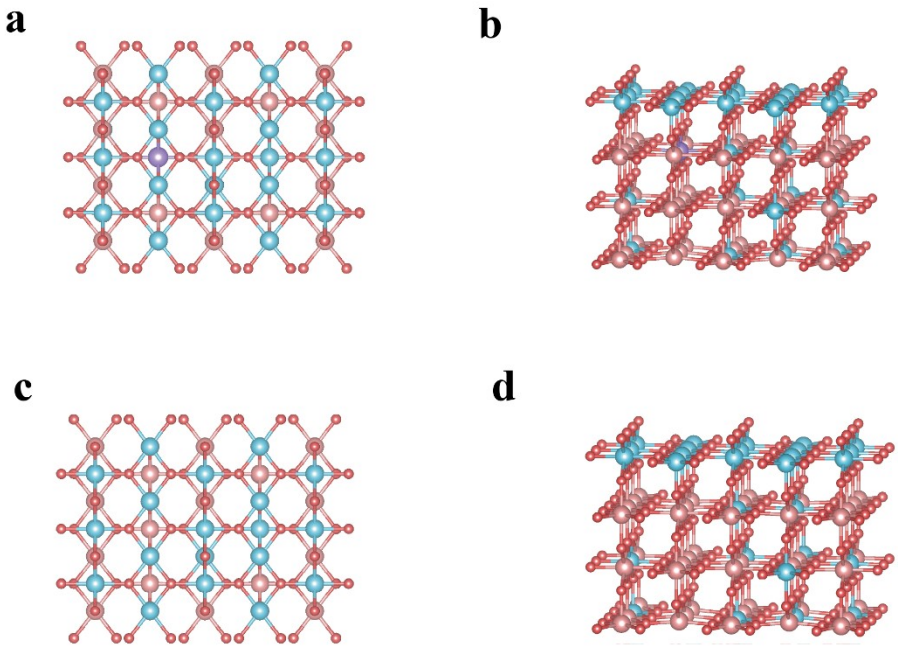

Figure S14. Schematic illustrations of the core-shell catalyst structures: （a, b) Top and side views of 5% Ta-doped IrRuOx@IrOx; (c, d) Top and side views of pristine IrRuOx@IrOx.

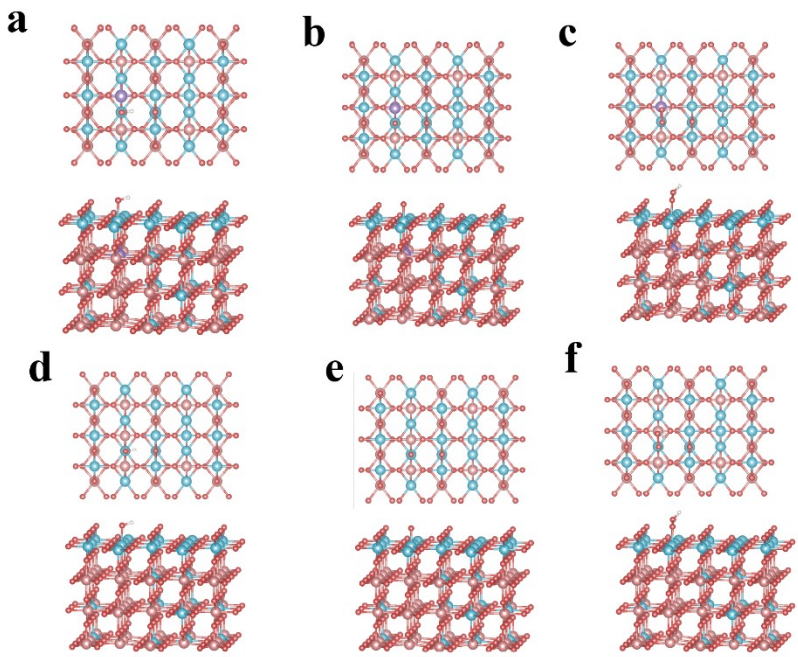

Figure S15. Schematic illustrations of reaction intermediate transfer at the core-shell interface: （a–c) Top and side views of 5% Ta-doped IrRuOx@IrOx; （d–f) Top and side views of pristine IrRuOx@IrOx.

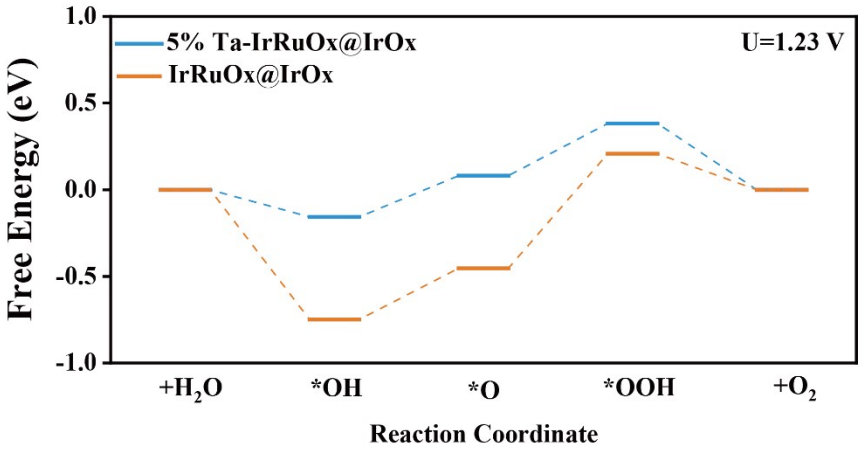

Figure S16. Free energy diagrams of the oxygen evolution reaction (OER) for 5% Ta-IrRuOx@IrOx and IrRuOx@IrOx catalysts at the equilibrium potential (U = 1.23 V).

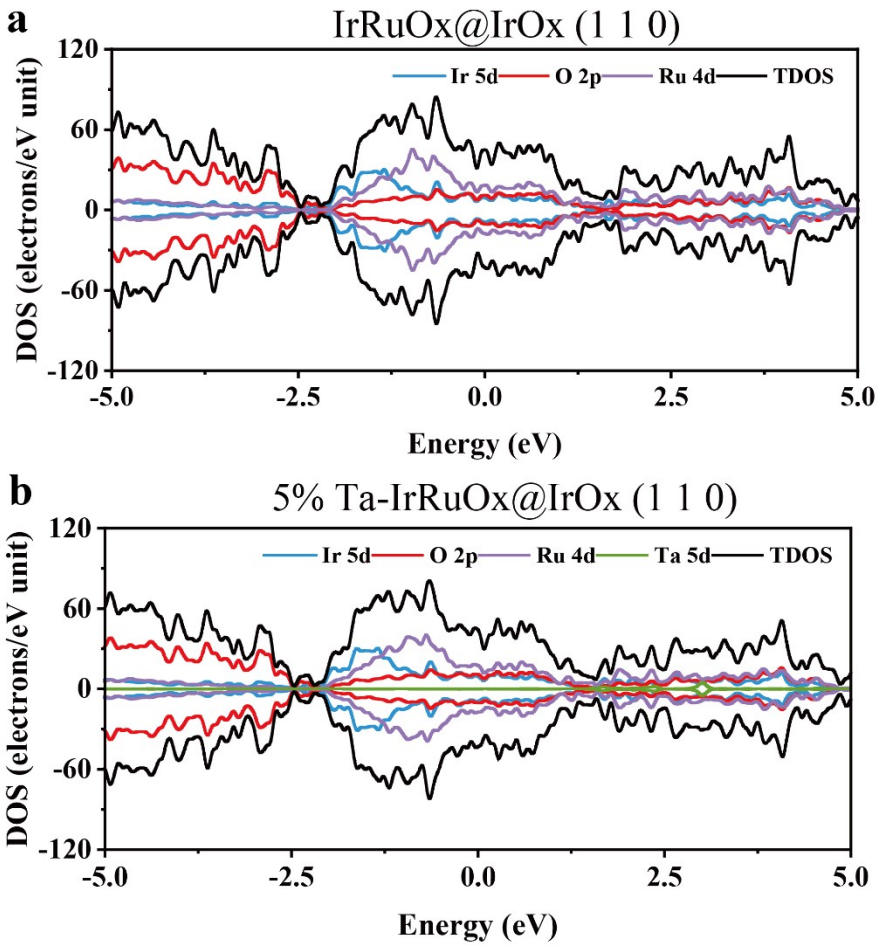

Figure S17. Density of States (DOS) calculations for the (1 1 0) facet: (a) IrRuOx@IrOx, showing Ir 5d, O 2p, Ru 4d, and total DOS (TDOS); 9b) 5% Ta-doped IrRuOx@IrOx, showing Ir 5d, O 2p, Ru 4d, Ta 5d, and TDOS.

Table S1. Bader charge analysis results of Ir and Ru atoms in the (1 1 0) planes of 5% Ta-IrRuOx@IrOx and IrRuOx@IrOx, showing valence electrons, total charge, and Bader charge values.

Sample		Valence electrons	Total charge	Bader
5% Ta-IrRuOx@IrOx (1 1 0)	Ir	9	7.5324	1.4676
	Ru	14	12.3262	1.6738
IrRuOx@IrOx (1 1 0)	Ir	9	7.4862	1.5138
	Ru	14	12.2708	1.7292

Table S2. Summary of the extended X-ray absorption fine structure (EXAFS) fitting parameters for 5% Ta-IrRuOx@IrOx and Ru foil, including coordination number, Debye-Waller factor, energy shift, bond distance, and reliability factor (R-factor).

Sample	Path	CN	σ^2	R	R-factor
5% Ta-IrRuOx@IrOx	Ru-O	2.10	0.00545±0.0011	2.02108 ±0.00959	0.0088165
	Ru-Ir	2.20	0.00588±0.0010	3.43682 ±0.0138	
	Ru-O	2.10	0.01378±0.00454	3.82408 ±0.00104	
Ru foil	Ru-Ru	6	0.00326±0.0004	2.66856 ±0.0028	0.0137561
	Ru-Ru	6	0.00871±0.0131	3.77262±0.0131	